JOURNAL OF MATERIALS SCIENCE 29 (1994) 6341–6353

Review
Crack growth in elastically damaged materials

F. E. BURESCH†*
Institute for Computer Applications, University of Stuttgart, Germany

A sudden heart attack ended the life and work of my father, on Friday 27 August 1993. This paper was found almost finished on his computer. The last corrections were done just a few hours before his death. It is dedicated as a farewell paper and legacy to all friends and colleagues, in his memory.

Dr Isabell Buresch.
Wieland Werke AG, Ulm, Germany
27 September 1993

Brittle, polycrystalline and polyphase materials such as ceramics and fibre-reinforced brittle composites contain residual thermo-mechanical stresses from manufacturing. These stresses are concentrated at sites of microstructural inhomogeneities such as grain and phase boundaries. The nucleation and growth of microcracks can minimize the local micro-strain energy density; thus, the local, residual stresses can act as nuclei for microcracks. The density of nuclei, statistically distributed within the material, depends on grain size, i.e. the distance between nuclei, with defined values of micro-strain energy density, is material specific. Stress-induced microcracking can act as an attractor for elastic damage at the local scale to produce a process zone that acts as a sink of strain-energy release on a larger scale, for example, the process zone at a crack front. It can be shown that the stress-rate dependent growth of local damage follows a power law which quantifies strengthening and softening during slow crack growth, prior to catastrophic crack extension. The damage-induced zone, produced by the release of strain energy on the local scale, can shield the macrocrack and grow to a critical value at the failure load. The influence of the microstructure on damage will be quantified and related to sub-critical and critical crack extension in brittle materials.

1. Scope

It was the intuition of Griffith [1] to develop a free-energy expression for the extension of a slit crack of length $2a$, in the field of a uniform uniaxial tensile stress, σ, that sums the decrease in mechanical energy (strain energy plus work done by the external load) with the crack's thermodynamic surface energy $4\gamma a$. He stated that spontaneous crack extension will occur when the differential of the free energy expression is less than or equal to zero. This insight leads to the well-known fracture equation

$$\sigma_c = Y\left(\frac{2\gamma E}{a}\right)^{1/2} \quad (1)$$

where Y is a numerical constant related to the specific type of crack and loading direction, E is Young's modulus and σ_c is the ultimate stress. Griffith nearly verified Equation 1 with the dynamic fracture of glass, where he experimentally determined that

$$a\sigma_c^2 = \text{constant} \quad (2)$$

Glass can be considered a nearly homogeneous material with inhomogeneities in the size scale of < 1 nm. Such inhomogeneities do not significantly influence the crack path. However, during fracture of most other brittle materials, the measured values of energy dissipation rate, G_c, can be more than one order of magnitude greater than the specific surface energy, i.e. $G_c > 2\gamma$. The size scale of heterogeneities in this class of materials is between 0.1 μm and 1 mm. Thus, the crack path becomes microscopically very tortuous with the production of a highly distorted material along the fracture surface. The difference between G_c and γ indicates the influence of the distortion produced by a non-linear, elastic deformation and irreversible shape changes within a process zone.

To quantify the observed high-energy dissipation rate during fracture, Neuber [2] and Irwin [3, 4] postulated, with the mean stress theory, a process zone of size $2w$ ahead of the tip of a crack. At the beginning of the seventies, it was recognized simultaneously by Hoagland and Hann [5] and the present author [6, 7]

* Any correspondence should be sent to Professor F. F. Lange, Materials Department, ENG III, University of California at Santa Barbara, Santa Barbara, CA 93016, USA.

0022–2461

that the process zone is a consequence of stress-induced microcracking due to the release of thermo-mechanical mismatch strains which arise at phase and grain boundaries within brittle materials during fabrication. The size of the process zone, $2w$, and the fracture energy, G_c, are material-specific parameters. They become critical at a material state which is related to a critical strain energy density given by

$$\left(\frac{dU}{dV}\right)_c = \frac{\sigma_{mc}^2}{2E} = \frac{G_c}{2w_c} \quad (3)$$

σ_{mc} was introduced by Neuber [2] as the notch fracture strength or the cohesion strength of the process zone. Physically, σ_m is the stress at which a critical state of the local damage exists within a zone of size $2w$, where favourably oriented, stress-induced microcracks coalesce with a macrocrack. By analogy, σ_m corresponds to the von Mises stress, as failure should occur as a consequence of dissipative processes. With the analogy to metals, failure occurs as a critical distortional strain-energy density absorbed by the material equals the energy density stored in the material loaded in uniaxial tension at yield. It was found experimentally, as well as theoretically, that σ_{mc} corresponds to the tensile strength in uniaxial loading [6–9].

Thus, the strain-energy density in the process zone is composed of two parts, i.e. the distortional part associated with damage, and the volumetric part associated with Hookian elastic strain. The Griffith theorem characterizes the pure opening mode of crack extension due to the Hookian strain-energy density. Fracture in brittle, disordered materials arises when the ratio in Equation (3) becomes critical, that is, as $w \to w_c$, which happens at a minimum value of the strain-energy density as reported by Sih [10]. With a critical notch fracture strength, σ_m, at the boundary of the process zone and the surrounding elastic material, the strain-energy release rate of a stationary crack, which is embedded in a local damage zone of stress-induced microcracks can be written as

$$G_c = \sigma_{mc}^2 \frac{2w_c}{E} \quad (4)$$

Stress-induced microcracking is the origin of the elastic damage; analogous to metals where deformation via dislocations produces plastic damage, microcracking and the opening displacements produced by the microcracking produces the elastic damage. Elastic damage becomes localized if stress-induced microcracking is confined to a highly stressed region which arises, for example, ahead of a crack or notch [8–17]. The microcrack-induced elastic damage reduces the effective axial Young's modulus inside the process zone to E_m. The elastic strain-energy density of the process zone after unloading is given as [12–17]

$$\frac{J_m}{2w} = \frac{\sigma_m^2}{2E}\left(\frac{E - E_m}{E_m}\right) \quad (5)$$

which is the crack-driving force during slow, stable crack growth in brittle materials. Equation 5 is the residual elastic strain-energy density stored in the microcracked process zone during stable crack growth [16, 17]. Similar effects were also reported by Atkins and Mai [15] during stable crack growth in adhesive joints.

Here, we will extend this work with a continuum mechanics analysis supported by experimental results concerning localized, elastic damage. It will be demonstrated that an elastic damage zone develops during stable crack growth in the strengthening range of a load–displacement curve for fracture mechanics specimens to the ultimate load, $P_{e\,ult}$, which is equivalent to a critical value of Equation 4. Physically, $P_{e\,ult}$ is a consequence of the elastic collapse within the damage zone, followed by elastic softening. The ultimate load can be defined as a bifurcation point due to the synergetic effect of damage and crack growth with a discrete jump of elastic strain-energy release rate during slow crack growth.

Thus, the relationship originally developed by Griffith between the strain energy release rate and the surface energy will be extended. The increase of the crack growth resistance during crack growth has to be related to the surface energy of multiple microcracks inside the damage zone of size $2w$. However, it is not only the increase of surface energy of the microcracks which contributes to energy dissipation. More important is the effect of the residual strains due to the cumulative, opening displacement of microcracks within the process zone, constrained by the surrounding elastic material. The effect of these residual strains at the boundary between the damage zone and the elastic material contributes to the rate of the elastic strain-energy density during stable crack growth. This will be explained in the following sections on the basis of the elastic–plastic beam theory in analogy to a double-cantilever beam (DCB), single-edge notch beam (SENB) and three-point bend specimens.

2. Elastic damage

2.1. Influence of localized, thermo-mechanical residual stresses

We will discuss elastic damage in some ceramics such as alumina, silicon nitride and C/SiC composites, with experimental results from the literature which were observed during fracture mechanics determinations with DCB and SENB specimens. The material properties and the experimental facilities are documented elsewhere [11, 16–28].

During the loading of a beam of a polycrystalline, brittle material (Fig. 1a) the displacement deviates from linearity if the load, P_e, exceeds at Y the load of the elastic limit, $P_e > P_E$ as shown in Fig. 1b [16, 17]. In brittle materials, stress-induced microcracking can be responsible for this non-linear effect. This arises if the superposition of the residual microstrain-energy density with the macrostrain-energy density reaches a critical value of the specific surface energy, 2γ, at a grain boundary of length $2a_m$ [12–14]. Thus, stress-induced microcracking takes place at specific

grain-boundary sites of length $2a_m$ and the elastic strain-energy density at the elastic limit is given by

$$\frac{\sigma_E^2}{2E} + \frac{\varepsilon^2 A^2}{24(1-\nu^2)} > \frac{\gamma}{a_m}. \quad (6)$$

The first term in Equation 6 represents the elastic strain-energy density of the external stress field, whereas the second term is due to the residual micro-strain-energy density at grain and/or phase boundaries; ε is the thermal mechanical strain $\Delta\alpha\Delta T$ where α is coefficient of thermal expansion and T is temperature. The parameter $A(0 < A < 1)$ is related to the crystallographic orientation of grains, and thus, the orientation of the microcrack [29]. Typically, the value of the residual strain-energy density is $\approx 3.6 \times 10^4\,N\,m^{-2}$, whereas the right-hand side of Equation 6 is $\approx 10^5\,N\,m^{-2}$ (e.g. alumina with a mean grain size of 10 μm). Thus, the elastic limit of Equation 6 decreases with increasing grain-boundary size, namely, microcracking arises first at sites in the microstructure with the lowest value of the microstrain-energy density, i.e. at grain boundaries where $a_m = a_{max}$.

To quantify the relations between the microcrack size, $2a_m$, and their relative separation distance, $x/2a_m$, we will assume that each facet or grain of size $2a_m$ is surrounded with a sphere of the same size which is embedded in an infinite matrix. Both spheres and matrix are assumed isotropic with common Young's modulus, E, and Poisson's ratio, ν. A penny-shaped crack is nucleated and arrests at the interface of the grain and the matrix. With these assumptions, we can estimate $x/2a_m$ with the following formula introduced by Koks [30]

$$\frac{x}{2a_m} = [(2\pi/3\beta)^{1/2} - \pi/2] \quad (7)$$

where β is the fraction of grain boundaries containing microcracks.

Specifically, in a single-phase, polycrystalline alumina [11–14, 16, 17, 22–26], at stresses not far beyond the elastic limit, the density of microcracks is relatively low because the fraction of the largest grains (size $2a_{max} = 40$ μm) is $\approx 1\%$ [25, 26]. At this state of damage, the relative distance between the largest grain boundaries is determined, with Equation 7 to be $x/2a_m \approx 13$.

Damage becomes localized when smaller grain boundaries $a_m < a_{max}$ become involved in the stress-induced microcracking process within the volume of

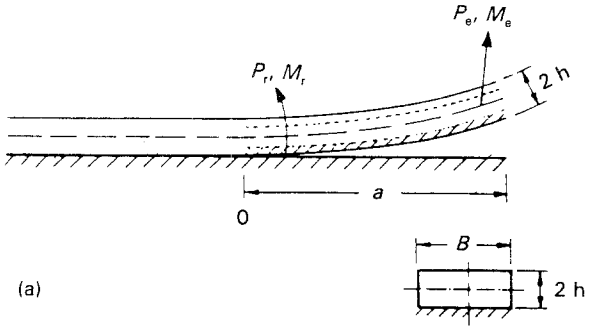

Figure 1 Deformation of an elasto-plastic beam: (a) Rotation of the elasto-plastic beam with thickness B and width $2h$. (b) Schematic load–displacement record with unloading at G at constant crack length a and after crack growth $a + \Delta a$ with elastic and inelastic displacement u_e and u_r.

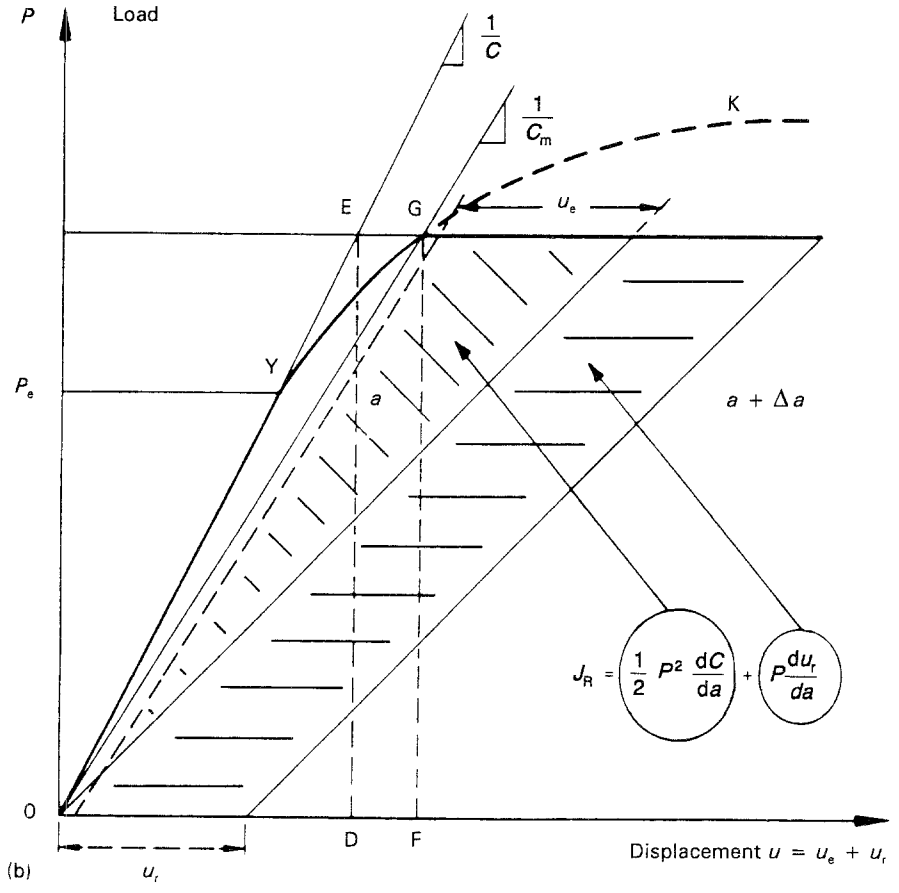

increasing strain-energy density [11–14] ahead of the macrocrack. The density of microcracks can increase to a critical value $\beta = \beta_c$. Specifically, this happens in the highly stressed elastic damaged outer strips of size $2w$ of the inhomogeneously loaded beam during strengthening, whereas the core of the beam deforms in an elastic manner (Fig. 1a) [16, 17]. Damage arises due to the release of the residual stress during stress-induced microcracking. This creates an inelastic strain contribution to the material's stress–strain behaviour. As proposed by Hutchinson [31], this inelastic uniaxial strain contribution increases with the external stress component, σ_{en}, normal to the plane of the microcracks as

$$\Delta\varepsilon = 16a_m^3\left(\frac{1-\nu^2}{3V}\right)\frac{\sigma_{en}}{E} \quad (8)$$

Using Equation 8 one can estimate the uniaxial dilation strain of a few nanometres for a 10 μm microcrack size by assuming a damage zone $V = V_m = 4 \times 10^{-11}$ m^3 and a strain of $\sigma_{en}/E = 10^{-3}$. Such an inelastic residual strain was experimentally qualified by Babilon *et al.* by small-angle X-ray scattering (SAXS) [18–22] and with acoustic emission analysis (AE) by Sklarczyk [23] who used SENB and DCB specimens of alumina. For a mean grain size of 10 μm, Fig. 2 shows the microcrack distribution ahead of a notch at a load above the elastic limit but before crack growth starts at a load P_0 with $P_E < P_e < P_0$ as a result of SAXS and AE measurements. The fractional microcrack density, β, increases to 120% with respect to the unstressed material at the edges of the notch, which had a width of $\approx$ 150 μm.

During stressing, both the zone size and the number density of microcracks at the crack tip were observed to increase during stable crack growth by SAXS [18–22], AE [23] and directly with a travelling microscope by Bärr [25, 26]. About 90% of the microcracks are oriented within an angle of 40° from the crack plane and were predominantly collinear aligned [18–22]. Favourably oriented microcracks coalesce during each step of incremental growth of the macrocrack when $x/2a_m \approx 2$. With these data and Equation 7, the critical microcrack density is determined as $\beta_c > 0.16$. The saturation arises after the initial crack grows $\approx$ 1 mm at the ultimate load. These data strongly suggest that the critical microcrack nuclei, β_c, is limited and agrees very well with foregoing numerical and experimental results when $\beta_c = 0.2$ [12–14].

At each instantaneous coalescence of microcracks, the strain-energy density (see Equation 5) is at a minimum and the microcracks close and would never be experimentally seen [25–28]. Thus, the growth of a microcrack is energetically quantified and jumps up by an incremental length, Δa, equal to the process zone, $\Delta a = 2w \approx 100$ μm for this specific material. Fig. 3 shows a sinusoidal-shaped damage zone after slow and rapid cracking observed by Frei *et al.* [27, 28] in a fine-grained alumina after microcrack decoration [32]. It shows a small damage zone during rapid crack growth and a wider damage zone during stable crack growth. In addition, the incremental crack growth with regions of high and low microcrack densities during slow crack growth are observed [32]. The incremental crack growth, Δa, is about three to five times the maximum grain size. Slow crack growth, in discrete incremental steps, with unloading–reloading events were also observed in graphite [33, 34].

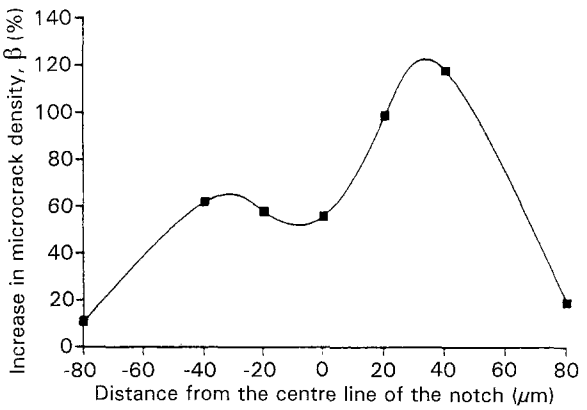

Figure 2 Distribution of relative increase of stress-induced microcrack density, β, in alumina ahead of a notch of width of 150 μm versus distance from the notch root mid-point at a load P_e with $P_E < P_e < P_0$ from Babilon *et al.* [22–24].

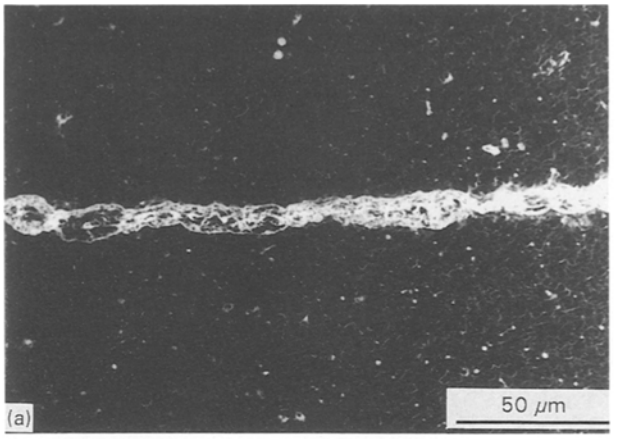

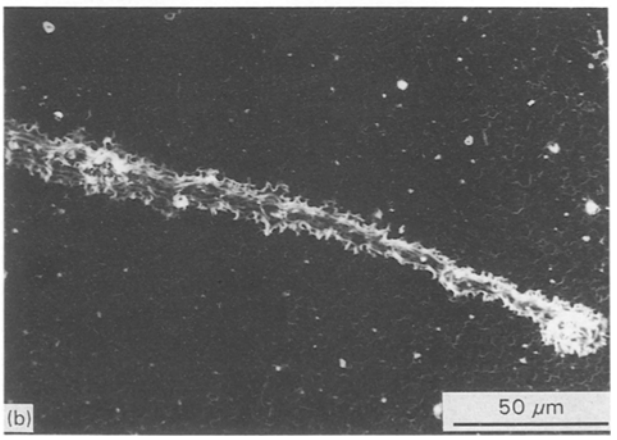

Figure 3 Decorated damage zones in a fine grained alumina (Buresch *et al.* [32]) in the wake of a stable and an unstable grown crack (Frei *et al.* [27, 28]) with large and small widths of damage zones.

Fig. 4 shows the microcrack density in the damage zone of alumina as a function of the residual crack-opening displacement as measured at different distances from the fracture surface (up to 240 μm) with SAXS. Fig. 5 shows the peak values from these SAXS measurements, illustrating that the size of the damage zone and the density of microcracks linearly decreases with the distance from the fracture surface and with increasing loading rate [12–14, 18–28, 33, 34]. During reloading (up to 80% of the initial load) the microcrack density distribution at different distances from the fracture surface is nearly constant. However, an additional elastic opening due to microcracks arises specifically in a range of about 5 mm behind the crack tip at distances larger than about 60 μm from the fracture surface.

The damage zone is divided into two parts. The inner zone, close to the fracture surface with a width of about 50–100 μm for the two different alumina ceramics, is unaffected by reloading. In the second part, i.e. for microcracks beyond 100 μm and up to 200 μm from the fracture surface, the microcracks are elastically opened by reloading. This division corresponds to the break of the slopes of the curves of Fig. 5. In the inner zone, Pangraz *et al.* [24] measured a reduction of the modulus of about 10%, whereas in the outer zone, the reduction is only 5%. Thus, the microcracks in the inner zone characterize the active damage zone which is shielded from the external stress field by the residual stress field of the damage zone.

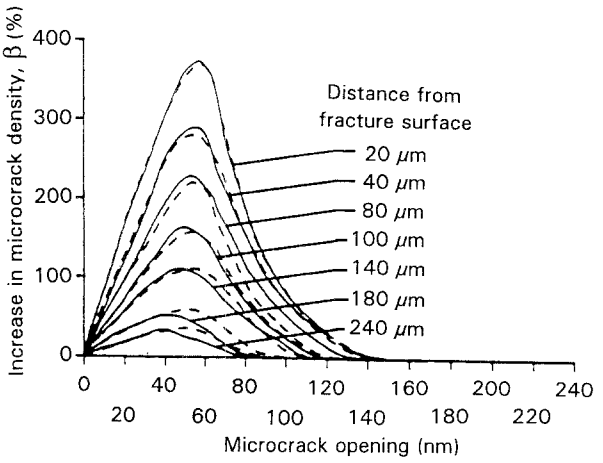

Figure 4 Frequency distribution of microcrack densities, β, in the damage zone of an alumina DCB specimen after (——), unloading and under (– – –) reloading [25, 26] at different distances from the fracture surface.

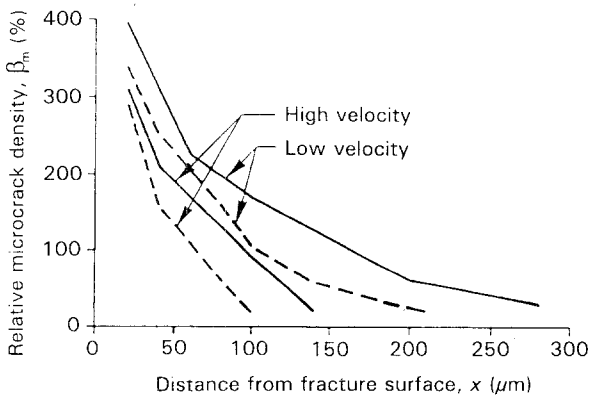

Figure 5 Influence of the crack velocity on the distribution of the relative increase of the stress-induced microcrack density, β, in the depth of damage zones and on the size of the total damage zone, R, of cracks in two aluminas with predominant intercrystalline and transcrystalline fracture versus distance from crack surface of (a) slowly and (b) rapidly growing cracks (Babilon *et al.* [22–24]). (——) AF997 intercrystalline, (– – –) B40 transcrystalline.

Thus, the size and the microcrack density of the damage zone of a stable growing crack are related to microstructural features such as the grain-size distribution. The characteristic length of a material connects sites with values of minimum micro-strain-energy densities (Equation 5) and influences the incremental crack growth and the size of the damage zone as pointed out by Sih [10]. Thus, failure of a material is a synergetic effect of the development of a damage growth and of crack growth as discussed in the next sections.

2.2. Local damage and residual stresses within the process zone

The stress-induced microcracking reduces the Young's modulus in the active, damaged zone to E_m and the compliance after unloading (see Fig. 1b). Thus, the unloading–reloading events in the damage zone during each incremental stable crack growth changes the strain-energy density and induces first-order residual strains $[(\sigma_m/E_m) - (\sigma_m/E)]$ on the boundary between the damage zone and the elastic material. The dissipated energy is stored partly as residual elastic strain energy in the damage zone given as

$$U_r = U_G - U_E = aB\sigma_m^2 \frac{2h}{E}\left(\frac{E - E_m}{E_m}\right) \quad (9)$$

where B is the body thickness, $2h$ its width, and a its length. It is assumed that the length of the beam corresponds to the length of the crack in a DCB specimen (Fig. 1a). Residual stresses also build up in the plastic zone during irreversible deformation of metals after unloading, as shown by Neuber [2], Atkins and Mai [15] and Pintschovius *et al.* [35].

In addition, it was shown that energy is dissipated during the irreversible straining of the process zone during stress-induced elastic damage

$$U_{diss} = B\sigma_m^2 w^2 \frac{a}{hE_m} \quad (10)$$

Thus, the area Oygf in Fig. 1b is the work which is done on the body during the elastic and inelastic deformation, which is

$$U_G = U_{el} + U_r + U_{diss} = B\sigma_m^2 \frac{aw}{3E}\left[\frac{h}{w} + \frac{3(E - E_m)}{E_m} + \frac{wE}{hE_m}\right] \quad (11)$$

Neglecting the third term when $h/w \gg 1$, the change of the critical strain-energy density with an incremental crack growth with respect to the damaged volume, $V_m = awB$, can be written, equivalent to Equation 5,

as

$$\frac{dU_G}{dV_m} = \frac{\sigma_m^2}{2E}\left[\frac{(E - E_m)}{E_m}\right]$$

$$= \frac{J_m}{2w} \quad (12)$$

The residual strain-energy density (Equations 5 and 12) of the process zone determines the flux of energy through the boundary of the damage zone and the elastic material, which is the characteristic length $2w$ and, in this case, the contour of the J-integral [36]. Thus, J_m is the effective driving force for the growth of a stable crack in brittle polycrystalline (and/or polyphase) materials [16, 17].

However, the residual elastic macrostrain-energy density of the damage front (Equation 12) corresponds to a dissipated residual microstrain-energy density. With the related surface energy, $2\gamma/a_m$ of an individual microcrack given as $\sigma^2/2E = \gamma/a_m$, it is reasonable to assume that the total dissipated microstrain-energy density increases linearly with the microcrack porosity, β, as

$$\frac{dU_r}{dV} = \frac{\gamma}{a_m}\beta \quad (13a)$$

This corresponds to Equation 8 introduced by Hutchinson [31] as the additional strain-energy density of a loaded microcrack is proportional to the related surface energy γ/a_m

$$\frac{dU_r}{dV} = \sigma_{en}\frac{\Delta N}{N}$$

$$= \frac{16}{3}\beta(1 - \nu^2)\frac{\gamma}{a_m} \quad (13b)$$

In the current notation, the scaling factor $16/3$ $(1 - \nu^2)$ in Equation 13a is not present. With this simplification, the rate of the dissipated microstrain-energy density on the contour $2w$ follows as

$$J_r = 2\beta w\frac{\gamma}{a_m}. \quad (14)$$

Equivalence of the macro- and microstrain-energy densities yields, with Equations 12 and 14, the cohesion strength on the boundary between the damage zone and the elastic material as [16, 17]

$$\sigma_m = I_m(2\gamma E/a_m)^{1/2} \quad (15)$$

where I_m is the crack-tip shielding function. I_m increases with the microcrack density, β, and the reduced Young's modulus, E_m, as is shown in Fig. 6

$$I_m^2 = \beta\frac{E_m}{E - E_m} \quad (16a)$$

or after some rearrangement

$$I_m = \frac{\sigma_m(\pi a)^{1/2}}{K_0}$$

$$= \frac{K_m}{K_0} \quad (16b)$$

where $K_m = \sigma_m(\pi a)^{1/2}$ and $K_0 = (2\gamma E)^{1/2}$ are the stress-intensity factors of cracks with and without a microcracked, process zone. With respect to microcrack systems of parallel and collinear oriented cracks, Equation 16a gives a good correlation with values from the literature [16, 17]. With Equations 15 and 16, the microcrack density can be described with

$$\beta = I_m^2\frac{E - E_m}{E_m} \quad (17)$$

or substituting Equation 16 as

$$\beta = \sigma_m^2\frac{a}{K_m^2}\left[\frac{E - E_m}{E_m}\right] \quad (18)$$

Physically, σ_m corresponds to the strength of a Griffith-crack multiplied with I_m. σ_m decreases with increasing grain size and increases with I_m. In addition, σ_m increases with the density of parallel oriented microcracks [12–14, 16, 17]. This beneficial effect on the toughness was also pointed out by Hutchinson [31]. In the limit of a non-damaged material, $\beta \to 0$ and $I_m \to 1$ [16, 17]. Thus, by combining Equations 12–16 with Equation 5, the strain-energy release rate,

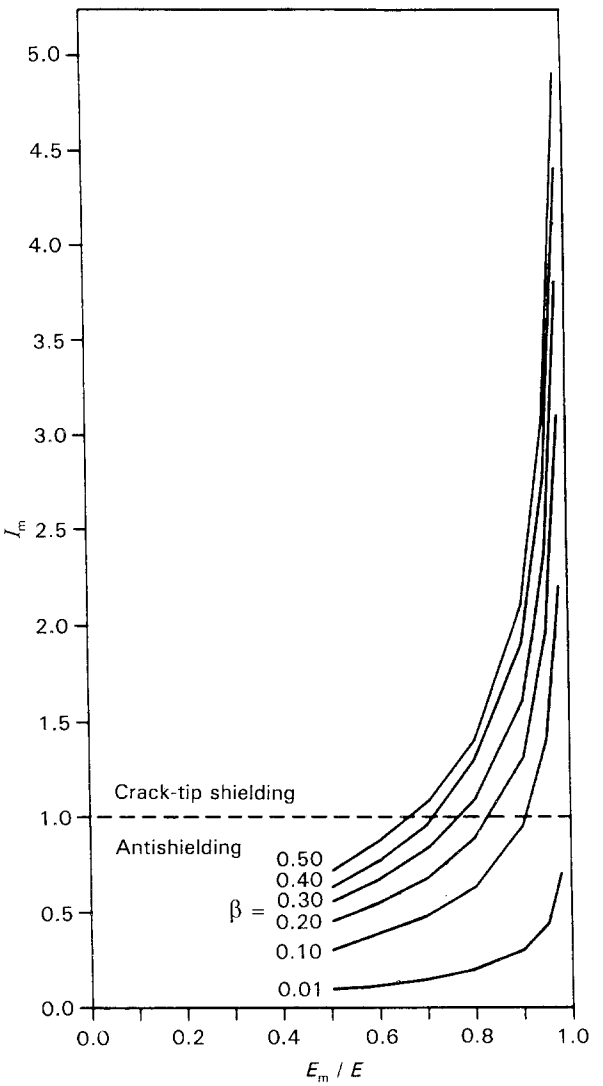

Figure 6 Crack-shielding function for uniaxial loading $I_m = \beta E_m/(E - E_m)$ versus related reduced Young's modulus, E_m/E, with the density β, of normal oriented microcracks as the parameter (Equation 16).

at the microscale of a stationary crack can be expressed as

$$J_R = wI_m^2 \frac{2\gamma}{a_m} \quad (19)$$

However, during crack growth, the rate of the residual strain-energy density increases due to the inhomogeneous growth of the damaged zone, which can be characterized by the tearing modulus $T_J = dJ/da$. Thus, during the steady-state growth of the crack the energy release rate at the microscale is expressed as

$$J_R = wI_m^2 \frac{2\gamma}{a_m} + w\left[d\left(wI_m^2 \frac{2\gamma}{a_m} \right) \Big/ da \right] \quad (20a)$$

which can be restated, using Equation 13a, as

$$J_R = w\left(\frac{K_0}{K_m}\right)^2 \frac{2\gamma}{a_m} + w\left[d\left(w\left(\frac{K_0}{K_m}\right)^2 \frac{2\gamma}{a_m} \right) \Big/ da \right] \quad (20b)$$

The first term on the right-hand side characterizes the opening mode of stable crack growth, whereas the second term is due to the rate in which the damage created by the microcrack zone dissipates the strain-energy density.

The distribution and strain-energy densities within the process zone and the localized, thermo-mechanical residual stresses in a microstructure are linked with the distortional strain energy per unit volume. This term characterizes the deviation from linearity of a load–displacement record which will be shown in the following section.

3. Damage growth and crack growth

3.1. Interpretation of load–displacement curves

As shown in the foregoing sections, failure of polycrystalline, brittle materials is governed by two rate processes, i.e. a dilatational effect due to crack growth (Equation 1), and a distortional effect due to the growth of a damaged zone (Equations 12 and 20b). The relative proportions of dilatation and distortion depend on the load history and location. Experimental, as well as theoretical, evaluations indicate that a local increase in damage due to microcracking can induce a critical assembly and interaction of microcracks which give rise to an incipiency of a macrocrack. Thus, growth of local damage due to microcracking can act as a prerequisite to crack growth whereby inhomogeneously distributed, non-local residual microstrains are partly converted into damage which induce residual macrostrains within the process zone.

The residual stresses in the local damage zone due to the anisotropic shape change of volume elements within the process zone of a growing crack are compressive inside and tangential tensile outside the zone. The residual stresses induce an internal bending moment in the specimen as the stress-induced microcracks build up a displacement discontinuity at the border of the zone ahead and in the wake of the stable growing crack. This is also observed for adhesive joints if residual stresses are built up during the joining process [15]. As a consequence, a residual compressive force, P_r, induces an internal bending moment, M_r, i.e. $M_r = aP_r$ with the crack length a and induces, in addition, a tangential, tensile stress at the crack surfaces. This was measured for an alumina ceramic with X-ray stress analysis by Mishima *et al.* [37]. Thus, as the internal bending moment induces an offset after unloading a cracked component, cyclic load–displacement curves for materials that experienced slow crack growth are characterized by a continuous shift of the elastic compliance. This is shown in Figs 7–9 for a fibre-reinforced composite of SiC (chemical vapour infiltration of SiC into laminated, carbon fibre cloth), a high-purity alumina at room temperature and a silicon nitride at 1200 °C, respectively [38–46].

As mentioned above, in the local elastic damage zone around a stably growing crack in brittle, polycrystalline materials, the effective axial Young's modulus is reduced by $\approx 10\%$. This is known for composites [47] as shown in Fig. 7, and was also measured with a scanning acoustic microscope (SAM) on a polycrystalline alumina [24]. The microcracks in bend specimens are highly oriented normal to the principal tensile stress which promotes agglomeration of favourable oriented microcracks to the macrocrack. This is first observed at the load, P_0, of a load–displacement record as depicted in Figs 7–9. With increasing external load above the load P_0, up to the ultimate load, P_{max}, a range is characterized by increasing damage, i.e. an increasing size of the damage zone and of the microcrack density. As shown in Fig. 9 for silicon nitride, the increasing damage induces an increasing residual compressive load, P_r, after unloading and an increasing residual offset, u_r. The ultimate load defines the critical damage state (CDS) [47] with a saturated microcrack density, $\beta \rightarrow \beta_c$.

Atkins and Mai [15] showed that P_r could be either graphically or numerically quantified by extending the local compliance lines of the loading–unloading loop to negative values. The crossing points define a specific crack length which is constant during each cycle. Extended compliance lines cross on the envelope which defines the locus of zero strain-energy release rate, G_R, of the material. The rate of the residual, compressive force, P_r, with crack length for silicon nitride at 1200 °C is shown in Fig. 10. This follows from Fig. 9 as subsequent local compliance lines of subsequent incremental crack growth cross at the curve of zero crack resistance, $G_R = 0$. At this curve, the external bending moment equals the residual bending moment, $M_e = -M_r$. The respective local compliance values follow with Equation 3 as $C_r = u_r/P_e$.

Thus, three areas can be specified under the load–displacement curve with respect to an incremental crack growth of Δa, which is shown in the insert of Fig. 9. These are two triangles and one trapezoid. The triangles are associated with the elastic strain energies of the external and the internal loads ($P_e u_e/2$) and ($P_r u_r/2$), respectively, and the trapezoid to the dissipated energy of the external load $P_e u_r$. The elastic and dissipated strain energy of a specimen, with thickness

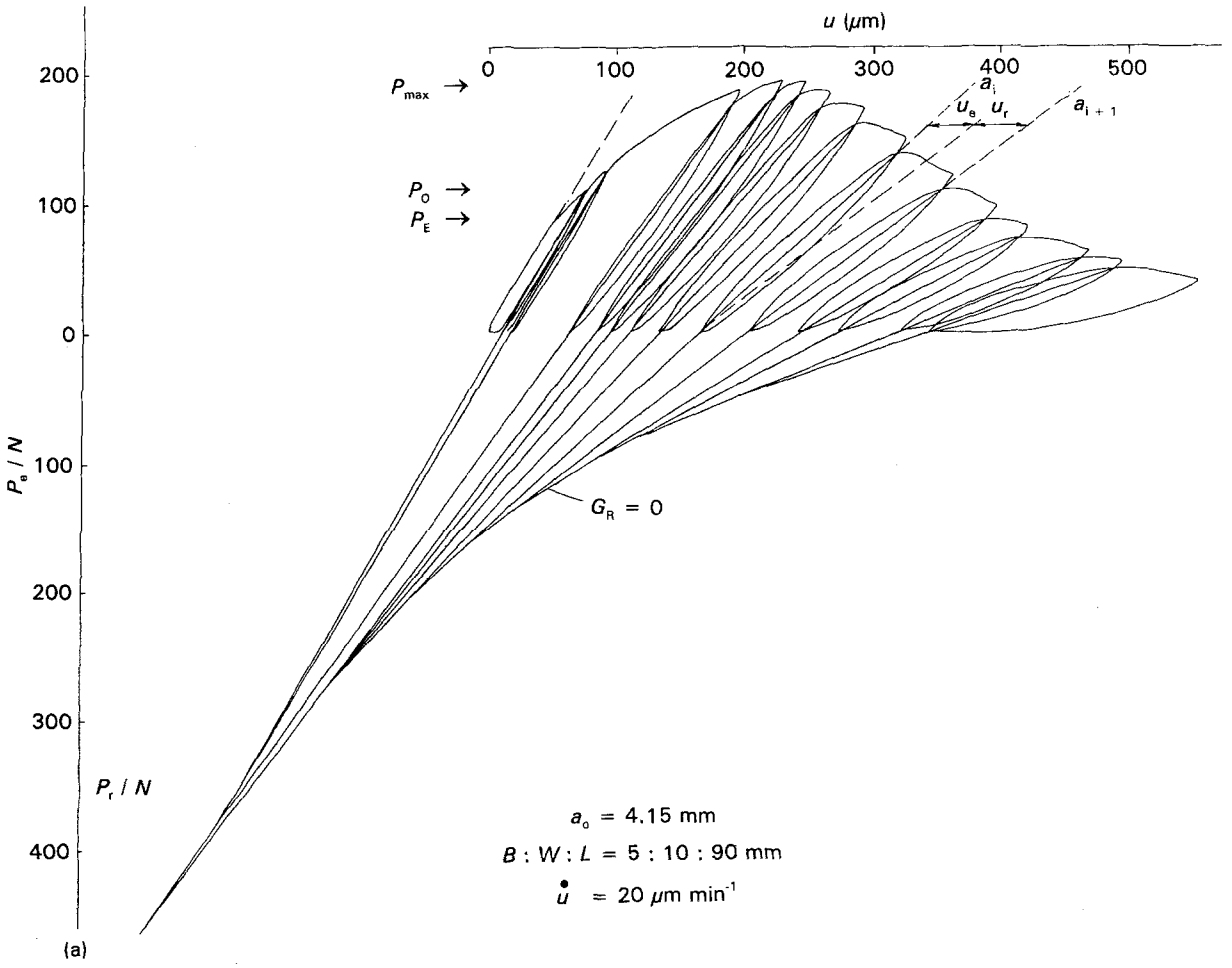

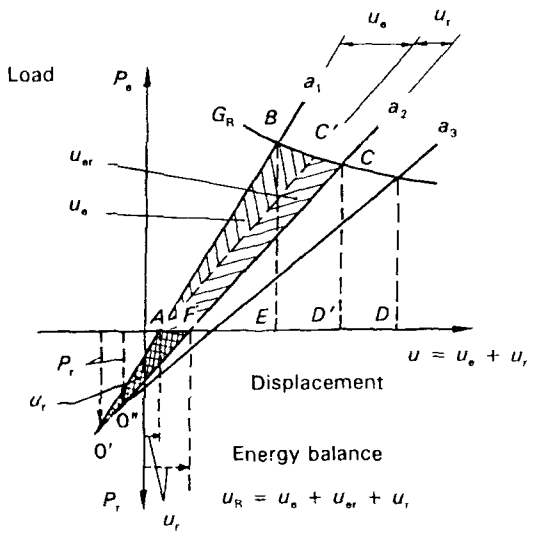

$$u_R = \frac{1}{2B} P_e u_r + \frac{1}{B} P_e u_r + \frac{1}{2B} P_r u_r$$

Figure 7 (a) Cyclic load–displacement record at room temperature of a C–SiC composite (Gomina *et al.* [43]) with extended compliance lines at constant crack length a. (b) Load–displacement record with incremental crack growth $\Delta a = a_{i+1} - a_L$.

B, is given by

$$U_R = \frac{P_e u_e}{2B} + \frac{P_e u_r}{B} + \frac{P_r u_r}{2B} \quad (21)$$

As proposed by Atkins and Mai [15] we describe the elastic, u_e, and the inelastic, u_r, displacements of a bend specimen with crack length, a, for the specific problem by

$$u = u_e + u_r = \frac{P_e a^3}{EI} + \frac{z a^n}{EI} \quad (22)$$

with the moment of inertia, I, and the power exponent, n, in the range $0 < n < 3$. To obtain a numerically tractable form of Equation 22 we substitute the power-law function

$$z = P_r a^{3-n} \quad (23)$$

and define with Equations 24 and 25 below, the macroscopic crack resistance, G_R, and a moment of crack resistance as a function of external and internal bending moments $M_e = P_e a$ and $M_r = P_r a$

$$G_R = \frac{3P_e^2 a^2}{2EI} + \frac{P_e P_r a^2}{EI} + \frac{P_r^2 a^2}{2EI} \quad (24)$$

which yields

$$M_R^2 = \frac{3}{2}\left[\frac{n}{3}(M_e + M_r)^2 + \left(1 - \frac{n}{3}\right) M_e^2\right] \quad (25)$$

The first and third terms of Equation 24 describe the opening mode of crack extension due to the dilatational strain energy, whereas the second term is a

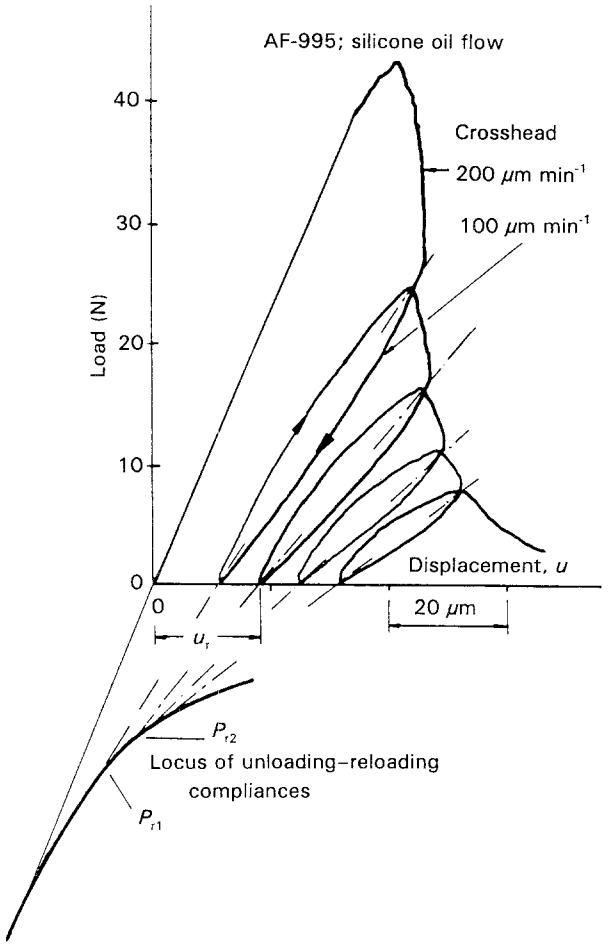

Figure 8 Cyclic load–displacement record at room temperature of an alumina (Osterstock *et al.* [11, 41, 42, 44]) with extended compliance lines at constant crack length, a.

consequence of the distortional strain energy and describes the damage of the process zone. The significance of the power exponent, n, is obvious from Equation 25 as the last term characterizes the dissipative work of the external force during damage by slow crack growth when $n < 3$.

At the maximum crack-growth resistance, namely $n = 3$, the last term of Equation 25 vanishes and the moment, M_R, instantaneously increases. Consequently, Equation 26 is well known, e.g. from Michener and Burns [48], and is only valid in the range of elastic softening with $n = 3$

$$M_R^2 = \frac{3}{2}(M_e + M_r)^2 \qquad (26)$$

The strengthening exponent n (< 3) quantifies the material-specific nucleation, growth and coalescence of stress-induced microcracks, i.e. the growth rate of damage which depends on the microstructure, loading rate and load history. Equation 24 is quadratic relative to the external and internal loads and can be solved for the related external load as

$$\frac{P_e}{P_r} = -\frac{n}{3} + \left[\frac{n^2}{9} - \frac{n}{3} + \frac{2}{3}\left(\frac{M_r^2}{G_r IEB}\right)\right]^{\frac{1}{2}} \qquad (27)$$

In the strengthening range of a stress–strain curve with $n < 3$, the compliance lines become relatively steeper with increasing crack length up to the ultimate

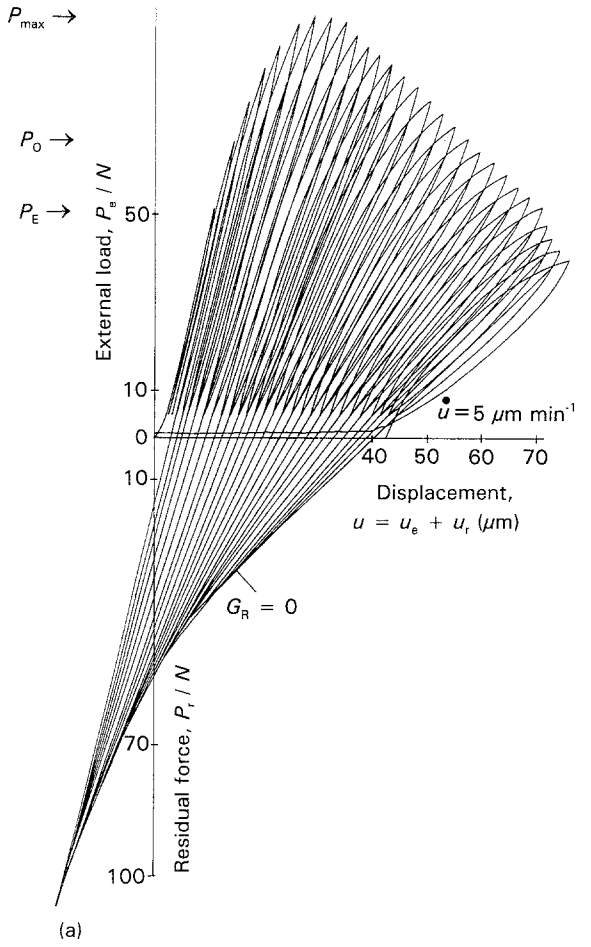

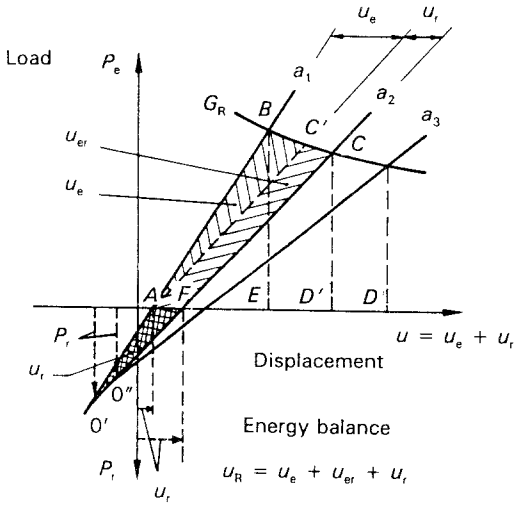

$$u_R = \frac{1}{2B} P_e u_r + \frac{1}{B} P_e u_r + \frac{1}{2B} P_r u_r$$

Figure 9 (a) Cyclic load–displacement record at 1200 °C of a silicon-nitride (Bodur [45, 46]) with extended compliance lines at constant crack length, a. (b) Schematic energy balance with elastic and residual displacements u_e and u_r at crack lengths a and $a + \Delta a$.

load as $n \to 3$. Thus, the crossing points of subsequent compliance lines during incremental crack growth cross during this stage at increasing residual loads, P_r, which are negative and caused by the dilation of microcracks within the process zone. In contrast, in the elasto-softening regime, with $n = 3$, the material behaves as an ideal linear elastic material and subsequent compliance lines cross with increasing crack

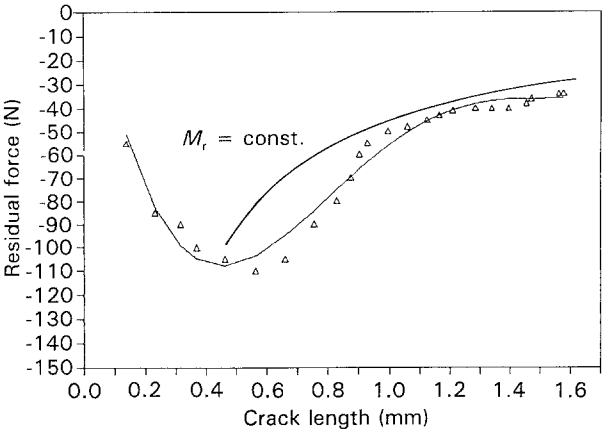

Figure 10 Residual compressive force P_r versus crack length a of silicon nitride at 1200 °C of Fig. 9.

length at smaller residual loads. Experimental evidence of this behaviour is reported for silicon nitride [45, 46] at high temperature and quantitatively for an alumina at room temperature [25, 26].

3.2. Crack-growth resistance

To optimize the performance of a component of a brittle material for a specific application and to reveal the influence of the microstructure on the failure, the crack resistance, G_R, must be quantified with respect to the macromechanical damage parameters. The damage parameters must be evaluated from the non-linear load–displacement curves for DCB and SENB specimens to quantify the dilatational and distortional terms, G_e and G_r, in

$$G_R = G_e + G_r = \left(\frac{P_e^2}{2B}\right)\frac{dC_e}{da} + \left(\frac{P_e}{B}\right)\frac{du_r}{da} \quad (28)$$

With unloading–reloading cycles, the external and residual load, P_e and P_r, the local elastic compliance, C_e, and the residual displacement, u_r, must be evaluated as a function of the increasing measured crack length. This procedure was used in evaluating the crack resistance of alumina at room temperature by Osterstock *et al.* [11, 44] and silicon nitride at 1200 °C by Bodur *et al.* [11, 38–40, 45, 46] using SENB specimen configurations.

The crack-resistance curves of Fig. 11 for alumina and Fig. 12 for silicon nitride show distinct maxima which correlate with the ultimate load where both the size of the damage zone and the microcrack density reach their critical values, i.e. at the minimum value of the strain-energy density (Equation 4). Also, at the maximum load, the moments of crack resistance change from Equation 25 to Equation 26. This change demonstrates a change in the rate-determining process, i.e. from strengthening by growth of the damage zone to elasto-softening by crack growth. Equivalent, with respect to Equations 22–26, evaluations of the residual offset displacement, u_r, as a function of crack length from the load–displacement curves are shown on the logarithmic scale in Fig. 13 for alumina. These curves demonstrate a break in the exponent at a crack length near the maximum load. Thus, experimental

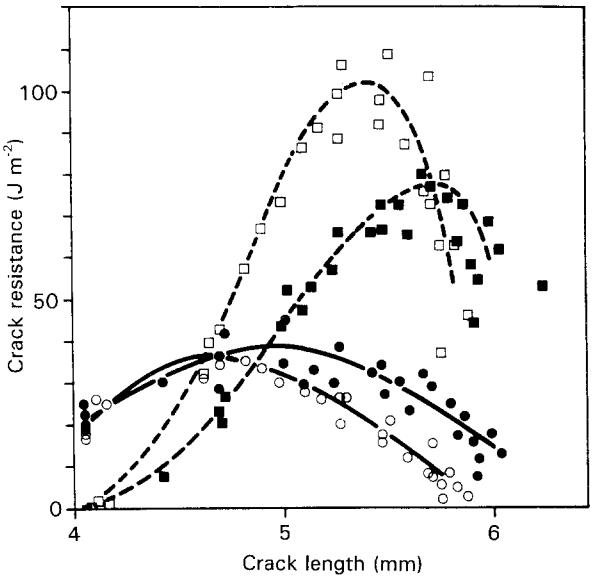

Figure 11 Elastic and residual crack resistance (—) G_e and (– – –) G_r (Equation 31) of an alumina versus crack length a (Osterstock *et al.* [44]). (□, ○) Safe/saine, (■, ●) 5 × 1090 °C.

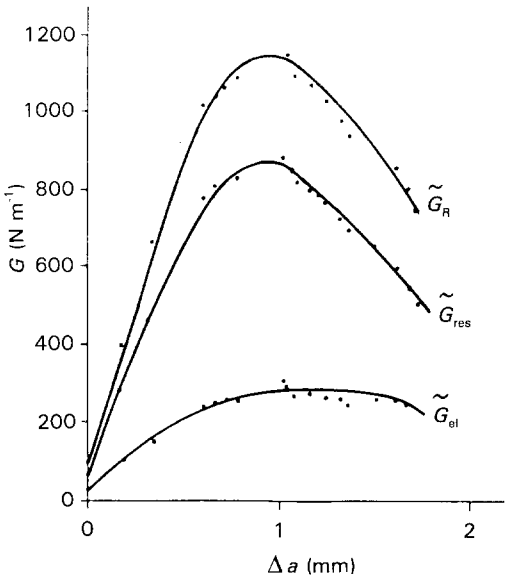

Figure 12 Crack resistance of silicon nitride at 1200 °C. $G_R = G_e + G_r$ with elastic and inelastic fractions G_e and G_r (Equation 31) versus crack length, a, evaluated from Fig. 9.

results show that before the maximum load, i.e. during strengthening, the exponent, n, in the power law Equation 20a is smaller than after the maximum load. The exponent is 3, beyond the maximum load in the case of alumina at room temperature, which indicates elastic softening as theoretically proposed in Equation 22.

The increase in crack resistance up to the maximum value is a consequence of increasing damage due to the distortional term, whereas the opening mode of crack growth seems to be slightly effected by damage. The ultimate load describes the critical damage state (CDS) with saturated damage as it follows experimentally

$$\frac{dG_r}{da} = 0 \quad (29)$$

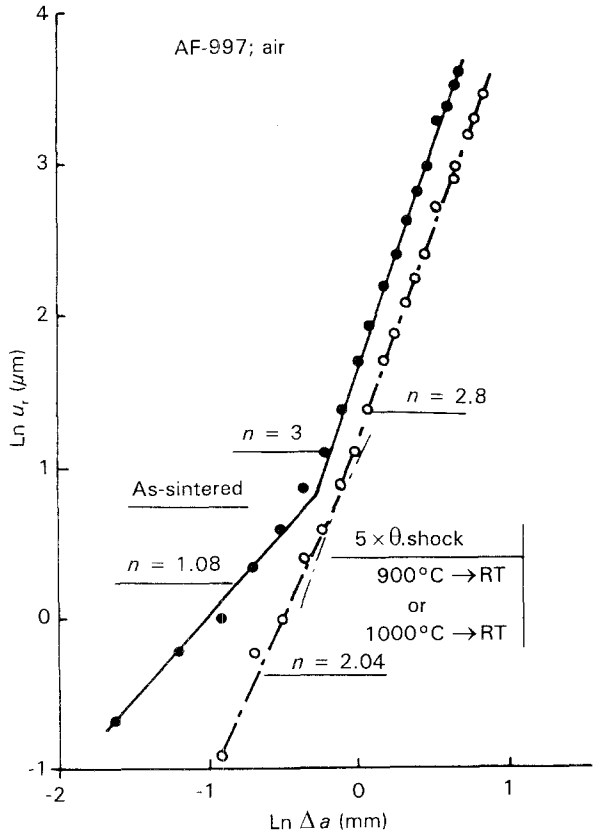

Figure 13 Residual displacement, u_r, of alumina versus stable crack growth in logarithmic scale with crack-growth exponent during elastic strengthening ($n = 1.08$) in the as-received state (high density of microcrack nuclei) and $n = 2.04$ in the pre-damaged state after thermal cycling (reduced density of microcrack nuclei), and during elasto-softening with $n = 3$.

at $n = 3$ and $P_e = -P_r$ (Equation 27). Physically, the ultimate load defines a bifurcation point as the elastic energy release rate increases during the break from the strengthening to the softening range by the amount of

$$\frac{\Delta G_R}{G_R} = \frac{3 - n}{4} \tag{30}$$

which follows from Equation 24.

4. Discussion

4.1. General remarks

Delayed failure of brittle disordered materials due to static or cyclic loading is a synergetic effect of two quasi independent phenomena, i.e. damage growth and stable crack growth. In the macroscale, non-local elastic damage starts at the elastic limit (Equation 6), i.e. at sinks of microstrain in a microstructure where there are statistically distributed nuclei for microcracks. Thus, in the microscale, the sinks of minimum values of microstrain energy are domains of maximum values of residual microstress concentrations which arise, for example, at triple points of the largest grain boundaries in polycrystals. Above the elastic limit, more and more microcrack nuclei arise, i.e. those with decreasing facet size a_m (Equation 6), to produce microcracks with an increasing local damage zone of size $2w$ (Equation 3). Thus, following the von Mises–Henky criterion, crack growth starts if the macrostrain-energy density (Equations 5 and 12) becomes critical and equals the strain-energy density induced in uniaxial loading at yield due to agglomeration of favourably oriented microcracks within the damage zone, namely, $J_m/2w = J_{mc}/2w_c$. The macrostrain-energy density $\sigma_m^2/2E = G_R/2w$ increases with increasing zone size, $2w$, up to the critical value $\sigma_{mc}^2/2E = G_{Rc}/2w_c$ (Equation 4) with an incrementally growing stable crack.

Stress-activated microcrack nuclei reflect the heterogeneity of the stress field in the material. The heterogeneity of the stress field results from the microstructure at grain and phase boundaries including reinforcements such as fibres. In the local damage zone, the stress field is homogenized and experimental results show that the microcrack field of the process zone in polycrystals is orthotropic as proposed by Sih [10]. The microcracks are predominantly oriented parallel to the macrocrack as revealed by Babilon *et al.* [18–22, 24] with SAXS measurements and also by direct microstructure observations [16, 17].

During increasing crack-growth resistance, up to a critical damage zone size $2w_c$, the damage zone with a maximum value of macrostrain-energy density of the global stress field the crack resistance reaches its maximum value, i.e. $(dU/dV)_c = G_c/2w_c$ (Equation 3). At this point, the residual compressive force within the process zone equals the external load $P_e = -P_r$. Then, the boundary of the process zone is free of normal stress as experimentally observed with photoelastic coatings of a graphite. It was found that the principal axis rotates by 90° during loading up to the maximum load [33]. Thus, the crack surfaces do not transfer normal stresses. This agrees with SAXS measurements because the elastic displacement of the opening of the microcracks inside the active damage zone of a crack with a length of 15 mm of a polycrystalline alumina during unloading–reloading is constant. Fig. 14 [18–22, 24] shows that inside the active damage zone, with a width of ≈ 100 μm, the elastic displacement of the microcrack opening is not influenced by reloading events. This crack-tip shielding effect of the

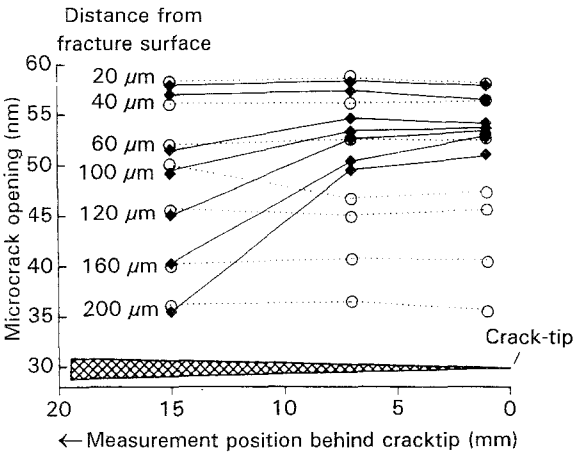

Figure 14 Infuence of an external load on the residual elastic opening-displacement (nm) of nominally normal oriented penny-shaped microcracks at different positions in the damage zone between 20 and 200 μm from the fracture surface and the length of the macrocrack in alumina (Bär [25, 26]). (◆) Loaded, (○) unloaded.

process zone is a consequence of stress-induced microcracking during crack-growth resistance as residual stresses due to microcrack opening displacement are built up during slow crack growth.

4.2. Crack-shielding phenomena

The foregoing continuum mechanics analysis and collaborating experimental results of polycrystals indicate that stable crack growth with increasing crack-growth resistance is governed by the principles of minimum values of strain-energy density (SED), i.e. a sequence of critical values of the dilatational and the distortional macrostrain-energy densities, dU_d/dV and dU_m/dV, during quantified stepwise stable crack growth. The strain-energy release rate during each incremental crack step (Equation 12) seems to be at a minimum and of the order of some Newtons per metre for large-grained alumina suggesting values of about $E_m/E = 0.9$ and $(\sigma_m^2/2E) = 0.1$ MPa [16, 17]. Non-local damage starts at the elastic limit. The elastic limit decreases with increasing grain size and increasing residual strain; Equation 6 is known from the literature for transformation-toughened ceramics [12–14, 16, 17, 48, 49] and also for cementitious materials [50].

The theoretical and experimental results indicate that the toughness increases during strengthening as the residual compressive force within the process zone increases (Equations 28 and 29) up to the ultimate load which defines a bifurcation point and the critical damage state (CDS) of a material at the maximum crack resistance. Thus, the crack-shielding function, I_m, reaches its maximum value as a consequence of a decreasing stress-intensity factor, K_m (Equation 16a) of the microcrack field due to parallel-oriented microcracks [18, 22, 24]. At the bifurcation point, the strain-energy release rate increases by an amount of $(3 - n)/4 < 1$ with respect to the energy release rate of stable crack growth during the "strengthening" range with $n < 3$ (Equation 33).

The beneficial effect of parallel-oriented microcracks on crack-tip shielding was also reported by Hutchinson [31] and others. However, our analysis shows clear evidence that the inventory of microcrack nucleation is limited because shielding is due to residual stresses which are built up during the stress redistribution processes by unloading/reloading events as a consequence of quantified incremental stepwise crack growth. This is bounded on the lowest level of strain-energy density which fulfils Equation 12.

At the ultimate load, as measured with polycrystals, the reduction of Young's modulus, E_m, in the active damage zone reaches its critical value of about $E_m < 0.9E$, which remains nearly constant during further slow crack growth [16–24, 47]. With this, we can physically interpret the toughness of a material as its ability to store a high density of metastable, pinned microcracks which is equivalent to the initial, residual strain-energy density associated with the grain/phase boundaries. The microcracked zone can also be viewed as lowering Young's modulus at the crack front, to enhance the strength of a Griffith crack (Equation 1) in elastically damaged materials [12–14, 16, 17]. Thus, it can be stated that the toughness of material increases with increasing density of microcrack nuclei. This is measured in composites, which are very heterogeneous [12–14, 16, 17], such as fibre-reinforced or transformation-toughened ceramics with a very heterogeneous microcrack structure [48, 49].

Obviously, the aforementioned experimental results seem to indicate that a crack does not transfer normal stresses, e.g. via bridging the macroscopic crack surfaces during the elasto-softening range as the boundary of the damage zone is elastically unloaded. This was also proposed by Bui and Ehrlacher [36]. Thus, the experimental results make it evident that the microcracks at the crack front and in the wake are elastically shielded by the residual stress field of the damage zone. With a maximum external force of 40 N of the load–displacement record for the alumina of Fig. 14 and a size of the process zone of $2w_{max} = 100$ μm [16], the notch fracture strength, σ_m (Equation 14) at the crack tip reaches values in the range of some gigapascals. This high shielding strength was also evaluated in a previous work using energy consideration and is expressed by the parameter I_m which reflects a low K_m value. However, this depends on the density of microcrack nuclei that become stress activated. The inventory of microcrack nuclei of a material increases with the heterogeneity of the microstructure which is equivalent to a decreasing value of the power-law exponent, n, in the range of $0 > n > 3$. If this density decreases, as measured by Osterstock *et al.* [11, 41, 42, 44], e.g. due to stress-induced non-local microcracking during thermal cycling, the compressive strength equivalent to σ_{mc} and the crack resistance also decrease and n increases, as reported above. However, the shielding effect holds only if the moment of inertia of the specimen is large enough to initiate the effective load-bearing capacity that withstands the residual stresses of the damage zone.

5. Conclusion

The importance of the microcracked process zone is two-fold. It is a safety factor as it stabilizes a crack, but homogeneous microcracking itself lowers strength. To optimize a microstructure for a specific application, it is important to optimize the standard deviation of the distribution of the microcrack nuclei and their local strain-energy density, that is, optimizing the grain- and phase-size distributions and their differential properties that give rise to the microstrains at grain and phase boundaries, all of which optimize the size of the process zone. Relations between stress-induced microcracking and redistribution of localized residual stresses to the process zone must be made more quantitative to predict static fatigue from microstructural parameters for this class of materials.

References

1. A. A. GRIFFITH, *Phil. Trans. R. Soc. (Lond.)* **A221** (1920) 163.
2. H. NEUBER, *Z. Konstruktion* **20** (1968) 245.

3. G. R. IRWIN, in "Handbuch der Phisik", Vol. 6, edited by S. Flugge (Springer, Berlin, 1958) pp. 551–60.
4. G. R. IRWIN and P. C. PARIS, in "Fracture", Vol. 2, edited by H. Liebowitz (Academic, NY, 1971).
5. R. G. HOAGLAND, G. T. HAHN and A. R. ROSENFIELD, *Roch. Mech.* **5** (1973) 77.
6. F. E. BURESCH, *Sci. Ceram.* **7** (1973) 383.
7. *Idem, ibid.* **7** (1973) 475.
8. *Idem*, in "8th Arbeitskr. Bruchvorgange" (DVM, 1976).
9. *Idem*, in ASTM STP 678, edited by S.W. Freiman (American Society for Testing and Materials, Philadelphia, PA, 1979) pp. 151–65.
10. G. C. SIH, *Theor. Appli. Fract. Mech.* **4** (1985) 157.
11. F. OSTERSTOCK *et al.*, Proj. MAE-0072-C, Final Rep., Lermat Cean, ESK Kempten, ICA Stuttgart, June 1991.
12. F. E. BURESCH, *Adv. Ceram.* **12** (1984) 306.
13. *Idem, Mater. Sci. Eng.* **71** (1985) 187.
14. *Idem, Mater. Pr.* **29** (1987) 261.
15. A. G. ATKINS and Y. W. MAI, "Elastic and Plastic Fracture" (Ellis Horwood, Chichester, 1985) p. 268.
16. F. E. BURESCH, "Lecture Notes in Engineering", No. 59, edited by K. P. Herrmann and Z. S. Olesiak (Springer, Berlin, 1990) pp. 227–38.
17. *Idem., Fort. Ber. DKG, Bd. 6. Heft* **1** (1991) 51.
18. F. E. BURESCH, E. BABILON and G. KLEIST, in "ICRS2" edited by C. Beck, S. Denis and A. Simon (Elsevier, London, 1989) p. 1003.
19. E. BABILON, G. KLEIST, F. E. BURESCH and H. NICKEL, *Sci. Ceram.* **14** (1988) 665.
20. *Idem*, in "ECF7" (1989) p. 552.
21. E. BABILON, K.K.O. BÄR, G. KLEIST and H. NICKEL, in "Euram Ceramics", Vol. 3 (Elsevier, 1989) p. 247.
22. E. BABILON, personal communication.
23. C. SKLARCZYK, *J. Eur. Ceram. Soc.* **9** (1992) 427.
24. S. PANGRAZ, E. BABILON and A. ARNOLD, *Acoust. Imag.* **19** (1992) 691.
25. K. BÄR, Dissertation, Aachen (1990).
26. K. BÄR, R. MERGEN and F. OSTERSTOCK, *Eur. Ceram.* **3** (1989) 190.
27. H. FREI and G. GRATHWOHL, Inst. Werkst. Uni. Karlsruhe, personal communication (1991).
28. H. FREI, G. PLAPPERT and G. GRATHWOHL, in "Euram Ceram", Vol. 3 (Elsevier, London, 1989) p. 115.
29. R. DAVIDGE, J. R. MCLAREN, I. TICHELL, *Frat. Mech. Cer.* **5** (1983) 594.
30. U. F. KOCKS, *Acta. Metall.* **14** (1966) 1629.
31. J. W. HUTCHINSON, *Acta Metall.* **35** (1987) 1605.
32. O. BURESCH, F. E. BURESCH, W. HÖNLE and H. G. VON SCHNERING, *Microchem. Acta (Wien)* **I** (1987) 219.
33. F. E. BURESCH, K. FRYE and TH. MÜLLER, *Fract. Mech. Ceram.* **5** (1983) 591.
34. F. E. BURESCH and H. NICKEL (DVM, 1984) pp. 123–34.
35. L. PINTSCHOVIUS, E. GERING, B. SCHOLTES, E. MACHERAUCH, 13.01. 01P05A, KFK (1988)
36. H. M. BUI and A. EHRLACHER, *Adv. Fract. Res.* **2** ICF 5 (1981) 533.
37. T. MISHIMA, Y. NANAYAMA, Y. HIROSE and K. TANAKA, *Adv. X-ray Anal.* **30** (1987) 545.
38. I. BURESCH and F. E. BURESCH, in "Third ICRS", Frankfurt (1993) in press.
39. F. E. BURESCH, *Fortschr. Ber. DKG Bd* **7** (1992) 140.
40. *Idem.* in "Proc. Third Int. Conf. Compu. Plasticity", edited by D. R. Owen, E. Onate, E. Hinton (1992) p. 1707.
41. M. GOMINA, D. THEMINES, J. L. CHERMANT and F. OSTERSTOCK, *Int. J. Fract.* **34** (1987) 219.
42. M. GOMINA and J. L. CHERMANT, *Fortschr. Ber. DKG Bd.* **3** (1988) 17.
43. M. GOMINA and M. H. ROUILLON, *ibid.* **5**(1) (1990) 283.
44. F. OSTERSTOCK and R. MOUSSA, *ibid.* **3** (1988) 71.
45. C. T. BODUR, Dissertation, Stuttgart (1989).
46. C. T. BODUR and K. KROMP, *Fortschr. Ber. DKG Bd* **3**(3) (1988) 109.
47. K. SCHULTE, in "18th Jahrestagung AVK", Freudenstadt, 6–7 October 1982.
48. J. R. MICHENER and S. J. BURNS, *Int. J. Fract.* **23** (1983) R45.
49. M. RÜHLE and A. G. EVANS, *Mater. Sci.* **13** (1989) 85.
50. F. E. BURESCH, in "Reliability of Engineering Materials", edited by A. L. Smith (Butterworth, London, 1984) pp. 55–74.
51. M. RÜHLE, N. CLAUSSEN and A. H. HEUER, *J. Am. Ceram. Soc.* **69** (1986) 195.

Received 20 January
and accepted 27 April 1994